Fuel 156 (2015) 96–102

Contents lists available at ScienceDirect

Fuel

journal homepage: www.elsevier.com/locate/fuel

Adsorption of Cu^{2+} on coal fly ash modified with functionalized mesoporous silica

Jaime Pizarro [a,*], Ximena Castillo [b], Sebastián Jara [b], Claudia Ortiz [c], Patricio Navarro [b], Héctor Cid [c], Héctor Rioseco [a], Daniel Barros [c], Nelson Belzile [d]

[a] Departamento de Ingeniería Geográfica, Facultad de Ingeniería, Universidad de Santiago de Chile, Santiago 9170022, Chile
[b] Departamento de Ingeniería Metalúrgica, Facultad de Ingeniería, Universidad de Santiago de Chile, Santiago 9170022, Chile
[c] Departamento de Biología, Facultad de Química y Biología, Universidad de Santiago de Chile, Santiago 9170022, Chile
[d] Department of Chemistry and Biochemistry, Laurentian University, Sudbury (Ontario) P3E 2C6, Canada

HIGHLIGHTS

- The waste material coal fly ash can be combined to a mesoporous material to adsorb metals.
- The synthesized compound is very efficient to remove Cu^{2+} ions from contaminated waters.
- The best conditions for the adsorption of Cu^{2+} have been investigated.

ARTICLE INFO

Article history:
Received 24 January 2015
Received in revised form 8 April 2015
Accepted 15 April 2015
Available online 23 April 2015

Keywords:
Coal fly ash
Mesoporous silica
Copper
Adsorption
Nanomaterials

ABSTRACT

The surface properties of coal fly ash modified with a mesoporous siliceous material and functionalized with 3-aminopropyl-triethoxysilane were studied to evaluate the adsorption capacity of the new matrix for Cu^{2+} ions under different pH, initial metal concentrations, number of contacts and times for different adsorbent masses. The synthesized material was characterized chemically and morphologically, showing an increase of active surface and pore uniformity with respect to the initial fly ash.

The new material showed great affinity for Cu^{2+}, whose removal was between 98% in the 10–20 mg L^{-1} initial concentration range, and 95% removal in the 30–45 mg L^{-1} initial range. At pH > 4, there was an increased adsorption capacity of the matrix, with pH 5 being the optimum working condition. The Freundlich model is the one that best represents the adsorption capacity of the studied matrix.

1. Introduction

The growing demand for energy at the world level has greatly increased the use of coal as a fuel for thermoelectric power plants, thus resulting in an increased accumulation of fly ash in the environment. India and China are two countries that have a large production of fly ash; it is estimated that India produces 140 million tons per year and that by 2015, China will be producing 580 million tons of fly ash yearly [1]. The accumulation of fly ash deteriorates the soil and becomes a source of emission of particulate matter to the atmosphere, thereby affecting air quality [2]. At the same time, it becomes necessary to mitigate the contamination of soil and water by metals introduced by anthropogenic activities to decrease the health risks to living beings and minimize the effects on natural ecosystems [3]. The growing accumulation of fly ash has lead to many studies aiming at developing possible industrial uses [4,5]. Fly ash has good metal adsorbing properties, and in view of its availability and abundance, it has become an interesting alternative material for the removal of the metals at low cost [6,7], in comparison with other technologies such as solvent extraction, chemical precipitation, separation through membranes, electrolytic processes, ion exchange, reverse osmosis, and biological systems [8,9]. In the area of new materials, numerous mesoporous materials (2–50 nm) based on silica have been synthesized and commercialized. These materials present several advantages such as high specific surface area, thermal and mechanical stability, uniform pore distribution, high adsorption capacity, and high functionalization ability [10]. Moreover, the adsorbing capacity of these materials and their affinity for some metal ions can be optimized by incorporating organic functions [11–16] on the surface and/or inside the pores. These nanostructures may constitute an effective alternative for the removal of metal ions from industrial effluents [17–20], in this way contributing to the recovery of

* Corresponding author. Tel.: +56 227182226.
E-mail address: jaime.pizarro@usach.cl (J. Pizarro).

http://dx.doi.org/10.1016/j.fuel.2015.04.030
0016-2361/

metals that have an economic value. Large mining activities in Chile generate a strong impact on the quality of the water used in the hydrometallurgical metal extraction processes [21]. The type of nanoparticles used in this study is an organic and silicon hybrid species that has a great surface/mass ratio and presents a better performance than zeolite as a porous material. This material is also known as MCM-41 [10].

The present study has the purpose of taking advantage of the two systems by synthesizing a new material using coal fly ash and a functionalized mesoporous material, and of evaluating the adsorption capacity for the removal of Cu^{2+} under different conditions of pH, initial metal concentrations, contact times, and maximum loads of the adsorbent material.

2. Materials and methods

2.1. Fly ash

The fly ash used in this study was class F and was obtained from a burning coal power plant located in Mejillones, Chile.

2.2. Synthesis

The synthesis of the matrix hexagonal mesoporous was obtained using the method of co-condensation [10] and it cannot be excluded that the hexagonal structure has been amended after the reaction with fly ash, which due to silicate content, would act as a precursor, enhancing the action of tetraethyl orthosilicate (TEOS). For the synthesis, 1.24 g of dodecylamine was first dissolved in ethanol (10 mL) and then 1.24 g of fly ash was added in 90 mL MilliQ (Millipore, Synergy UV) water while stirring at 1000 rpm. Then, 0.71 mL of the organosilane 3-aminopropyl-triethoxysilane (APS) and 6.09 mL of tetraethyl orthosilicate (TEOS) were added. After 30 s, 0.94 mL of the solvent 1,3,5-trimethylbenzene (TMB) was added and the mixture was stirred constantly during 24 h; it was then filtered and the solid was dried at ambient temperature. The TMB remaining in the synthesized matrix was Soxhlet extracted with ethanol (125 mL) during 5 h. The sample was then dried at ambient temperature during 24 h [10].

2.3. Physico-chemical and morphological characterization

Four analytical techniques were used for the physicochemical characterization of the fly ash and the synthesized matrix (fly ash modified with Hexagonal Mesoporous Silica (HMS) functionalized with 10% APS): Inductively Coupled Plasma/Optical Emission Spectroscopy, ICP-OES (Perkin Elmer Optima 2000) for the elemental composition of fly ash; scanning electron microscopy (SEM) (TESCAN Vega 3) with energy dispersive X-ray spectrometry (EDX) analyzer for a topographic analysis and quantification of components; Fourier Transform Infrared Spectroscopy (FTIR) (Spectrum Two IR Spectrometers, Perkin Elmer) for the determination of functional groups in a range of 4000–600 cm^{-1}, and surface area measurement by the BET method and pore size distribution by BJH (Micrometritics ASAP 2010).

2.4. Adsorption tests

To evaluate the affinity of the Cu^{2+} ion for the synthesized material, various adsorption tests were performed. The variables studied to evaluate the adsorption capacity of the matrix ($mg\,g^{-1}$) included the effect of the initial concentration of Cu^{2+}, adsorption pH, maximum load capacity of the synthesized material, and equilibration times for different adsorbent masses.

The reagents used to carry out the adsorption tests were either Analytical or Certipur grade. The contact solutions were prepared from a standard copper solution (Merck) of 1000 $mg\,L^{-1}$ of $Cu(NO_3)_2$ in 0.5 $mol\,L^{-1}$ HNO_3 and MilliQ water (Millipore, Synergy UV). The pH was adjusted with 0.1 M NaOH and 0.1 M HNO_3.

2.4.1. Adsorption isotherm

This test allows the adsorption capacity of synthesized material to be evaluated at different adsorbate concentrations in solution. The tests were performed by contacting 0.1 g of adsorbent with 5 mL of solution at 10, 15, 20, 30, 40, and 45 $mg\,L^{-1}$ of adsorbate at pH 5. The batch experiments were carried out in a 15 mL beaker, with stirring for 24 h at 150 rpm. The phases were then separated by passing through a membrane filter (0.22 μm), and the Cu^{2+} concentration at equilibrium was determined by flame atomic absorption spectrometry (FAAS, Thermo Scientific, iCE 3000 Series).

2.4.2. Effect of pH

The variation of the adsorption of Cu^{2+} as a function of pH modifies the surface charge of adsorbent (fly ash and synthesized matrix) and the distribution of species associated with the metal. To determine the optimum pH, 0.1 g of adsorbent in 5 mL of solution were placed in contact with a 30 $mg\,L^{-1}$ solution of the metal in the pH range 2.0–8.0.

2.4.3. Maximum load capacity

The maximum load of the matrix allows the determination of the effectiveness of the material at different contact times with a given Cu^{2+} concentration. To measure it, a 0.1 g sample of adsorbent was put in contact six times with a 30 $mg\,L^{-1}$ Cu^{2+} solution at the optimum adsorption pH during 60 min.

2.4.4. Adsorbent mass and contact time

Tests were done to determine the adsorption time at different adsorbent masses. The rate at which the metal was adsorbed was determined by putting in contact 0.5, 1.0 and 3.0 g of adsorbent with 50 mL of a 30 $mg\,L^{-1}$ Cu^{2+} solution at pH 5 during different stirring times (5, 10, 15, 20, 30, 60, 90, and 120 min).

3. Results and discussion

3.1. Physico-chemical and morphological characterization

The main elements contained in the used not modified fly ash were Si, Al and Fe at concentrations of 239.5, 108.0 and 60.3 $mg\,g^{-1}$, respectively (Table 1). The surface analysis by SEM

Table 1
Elemental composition of fly ash analyzed by ICP-OES.

Element	Concentration ($mg\,g^{-1}$)
Si	239.5
Al	108.0
Fe	60.3
C	60.0
K	14.0
Ca	13.0
Mg	6.2
Ti	5.7
S	3.9
P	0.8
V	0.3
Zn	0.2
Sb	0.2
Mn	0.2
Cu	0.19
Ni	0.14
Cr	0.1
Co	0.04

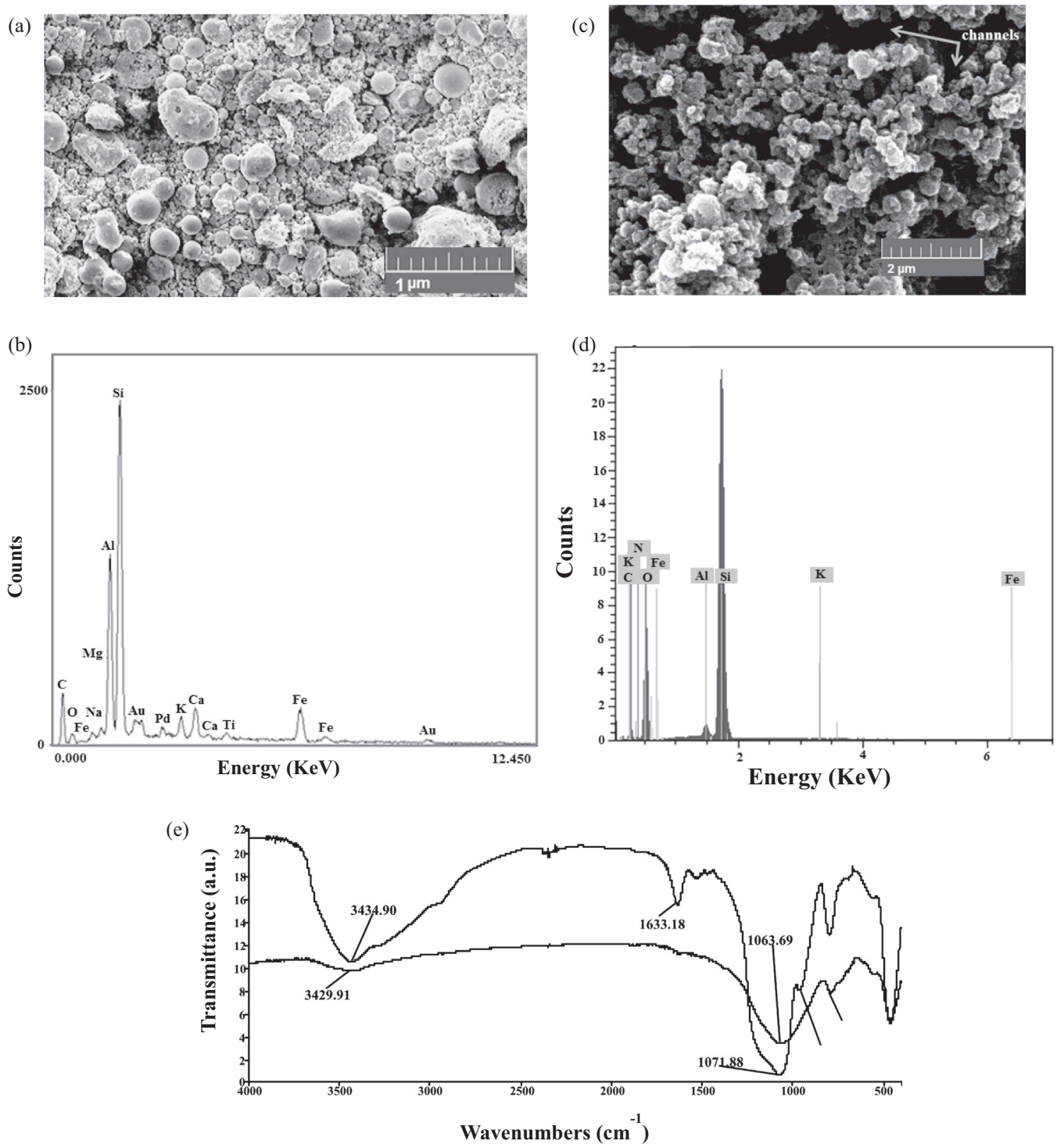

Fig. 1. (a) SEM of fly ash at 20 KeV; magnification 200×. (b) EDS elemental composition analysis of fly ash. (c) SEM of synthesized matrix at 20 keV; magnification 20 K×. (d) EDS analysis of elemental composition of synthesized matrix (e) FT-IR spectra: (a) fly ash (b) synthesized matrix.

showed that fly ash consists mainly of spherical particles with diameters between 10 and 100 µm, (Fig. 1a), with a high content of puzzolanic compounds such as silica (SiO_2) and alumina (Al_2O_3) giving the fly ash its vitreous character (Fig. 1b) [22].

The FT-IR spectrum of the synthesized matrix (Fig. 1e) shows a strong absorption band at 3450 cm^{-1}, associated with the O–H bonds of the silanol groups. The bands corresponding to the symmetric and asymmetric Si–O–Si vibrations are seen at 800 and 1090 cm^{-1}, respectively. After the functionalization with 10% (w/v) APS of the mesoporous matrix with fly ash, it is clear that the spectrum differs from the previous one, showing a wide signal between 3000 and 3600 cm^{-1} due to the increased number of silanol groups contributed by the mesoporous material itself, and stretching bands due to the N–H group of 3-aminopropyl-triethoxysilane, whereas the band at 1633 cm^{-1} corresponds to the bending vibration of the N–H groups (Fig. 1e).

The BET and BJH analyses of the fly ash, the ash modified with mesoporous material and functionalized with 10% APS

Table 2
Comparison of the BET and BJH analysis of functionalized HMS, fly ash, and synthesized matrix.

Analysis	Sample		
	HMS-NH_2 [24]	Fly ash	Fly ash + HMS + 10% APS
BET surface area ($m^2\ g^{-1}$)	17	19.77 ± 0.29	415.25 ± 0.19
BJH adsorption cumulative surface area ($m^2\ g^{-1}$)	–	14.25	479.84
BJH desorption cumulative surface area ($m^2\ g^{-1}$)	–	9.97	552.63
BJH pore volume (adsorption) ($cm^3\ g^{-1}$)	0.017	0.0152	0.535
BJH pore volume (desorption) ($cm^3\ g^{-1}$)	–	0.0136	0.602
BJH pore diameter (adsorption) Å	–	44.59	42.49
BJH pore diameter (desorption) Å	–	54.43	43.57

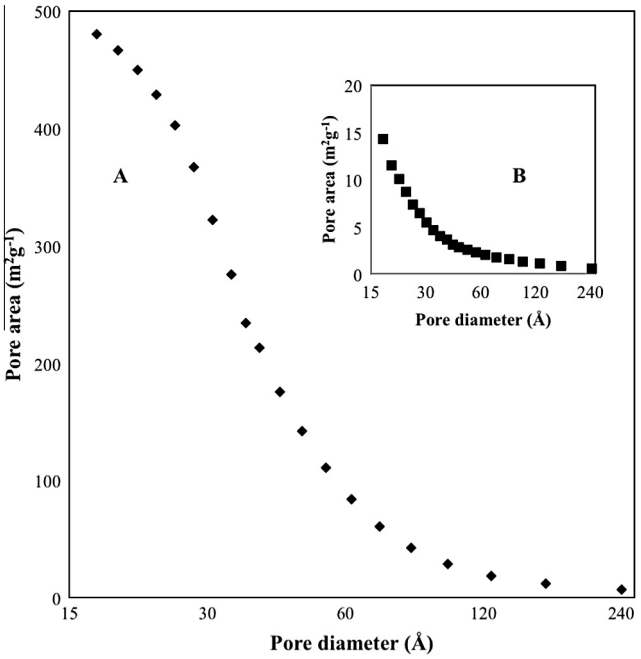

Fig. 2. Comparison of Pore diameter distribution as a function of pore area between synthetized matrix (a) and fly ash (b).

(synthesized material), and the mesoporous silica functionalized with primary amines are presented in Table 2, showing that the specific surface area of the synthesized material increased by more than 20 times compared to that of the non treated fly ash, i.e., from 19.77 ± 0.29 $m^2\ g^{-1}$ to 415.25 ± 0.19 $m^2\ g^{-1}$ in the synthesized material. The pore size distribution obtained by the BJH method showed an adsorption/desorption ratio of 42.49/54.43 Å for the initial fly ash, while for the synthesized material this ratio was 44.59/43.57 Å. The pore diameter and pore diameter ratio corresponds (Fig. 2a and b) to a mesoporous material, which according to the IUPAC classification [23] includes diameters between 20 and 500 Å. The pore diameter ratio found for the synthesized material points to an increased uniformity of the material with respect to the ash.

Fig. 1c shows size and structure of synthetized matrix, and their elemental composition (Fig. 1d). The composition indicates the presence of oxygen, silicon, carbon, nitrogen, aluminum, iron and potassium. The presence of nitrogen shown by this analysis as well as by FT-IR confirms the functionalization with the primary amine APS. Fig. 1c shows the increased uniformity of the surface of the synthesized material compared to the pure fly ash and the formation of channels that would confirm the increased porosity of the synthesized material, where the adsorption/desorption volume and the pore ratios show that we are indeed dealing with a functionalized mesoporous material (Table 2).

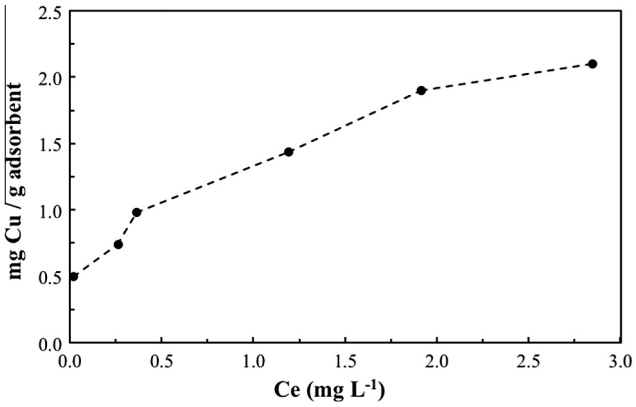

Fig. 3. Adsorption isotherm of Cu^{2+} of synthesized matrix.

3.2. Adsorption

3.2.1. Adsorption isotherm of the synthesized material

The adsorption isotherm of Cu^{2+} was studied using the synthesized functionalized mesoporous material. Fig. 3 shows the Cu^{+2} adsorption capacity of the synthesized material as a function of the equilibrium concentration. In the studied concentration range, the new material showed an affinity for the adsorbate that caused an increased adsorption capacity as the metal concentration increased to finally achieve approximately 98% removal of Cu^{2+} in the 10–20 mg L^{-1} initial concentration range, and 95% removal in the 30–45 mg L^{-1} range. The results of the BET analysis, showing significant increased pore volume and active surface, can explain the stunning increased adsorption capacity of the different initial metal concentrations.

The linear Langmuir and Freundlich adsorption models were fitted to the results of the Cu^{2+} adsorption equilibrium. The linear form of Langmuir's equation is given as [25]:

$$\frac{C_e}{q_e} = \frac{1}{q_L \cdot K_L} + \frac{C_e}{q_L} \quad (1)$$

where C_e (mg L^{-1} or ppm) correspond to the equilibrium concentration of the metal and q_e (mg g^{-1}) is the ratio between the mass of Cu^{2+} and mass of adsorbent at equilibrium. The constants q_L (mg g^{-1}) and K_L (L mg^{-1}) are the maximum adsorption capacity of the monolayer and the constant that relates to the adsorption free energy, respectively. In turn, the linear form of the Freundlich equation can be expressed as [26]:

$$\ln(q_e) = \ln(K_F) + \frac{1}{n} \cdot \ln(C_e) \quad (2)$$

where K_F (mg g^{-1}) (mg $L^{-1})^{1/n}$ and n are the Freundlich constants that relate to the adsorption capacity and intensity of the adsorbent for a given adsorbate, respectively. The values of the constants in both models are obtained from the slope and the position

Table 3
Values of the constants and fitting of the adjusted adsorption models.

Langmuir Model			Freundlich Model		
q_L (mg g^{-1})	K_L (L mg^{-1})	R^2	n	K_F (mg g^{-1}) (mg L^{-1})$^{1/n}$	R^2
1.31	28.78	0.747	3.31	1.41	0.937

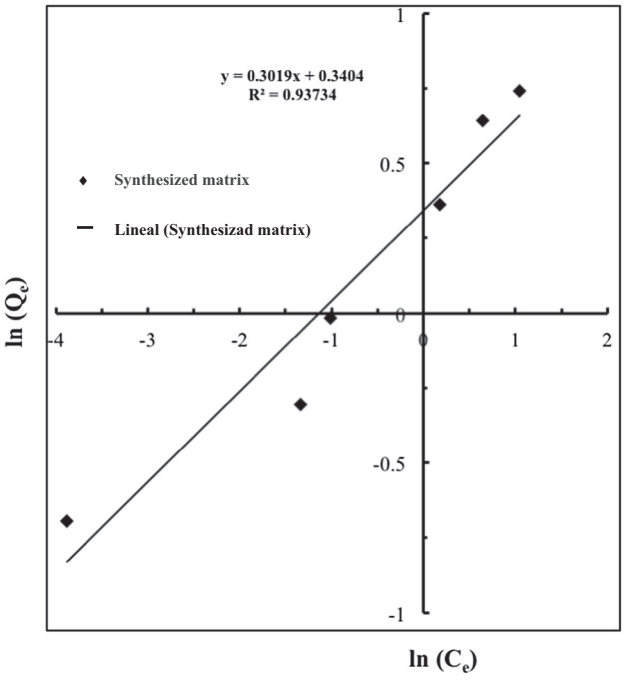

Fig. 4. Freundlich model fit of synthesized matrix.

coefficient of the linear fit to the adsorption equilibrium results. Table 3 shows the results of the fit and of the constants of both models. The Freundlich adsorption model, assuming that the surface of the adsorbent is a monolayer, shows a better fit with our experimental data (Fig. 4). The value of n was 3.3 for the studied system; if the value of n is between 1 and 10, the adsorption is considered favorable according to Slejko [27].

3.2.2. pH

The adsorption of Cu^{2+} in the synthesized material was analyzed and Fig. 5 shows the variation of the loading capacity (mg g^{-1}) as a function of pH. At pH < 4, both matrices present a low adsorption capacity due to competition between hydrogen ions and Cu^{2+} for the active sites of the surface adsorbent [28]; at pH > 4 the hydrogen ion concentration decreases, favoring the adsorption of Cu^{2+}, a phenomenon that is explained by the presence of oxides such as SiO_2, Al_2O_3, Fe_2O_3 and whose charge depend on the pH of the medium. The mechanism of exchange between hydrogen ions and the metal ions is represented by the following equations:

$$-XOH + H_3O^+ \rightarrow XOH_2^+ + H_2O \quad (3)$$

$$-XOH + OH^- \rightarrow XO^- + H_2O \quad (4)$$

$$2(-XO^-) + M^{2+} \rightarrow (-XO)_2M \quad (5)$$

X : Si, Al, Fe

M : metal

As pH increases, negative charges on the surface of the matrix increase thereby increasing the electrostatic attraction capacity between adsorbate and adsorbent [29,30]. The most efficient

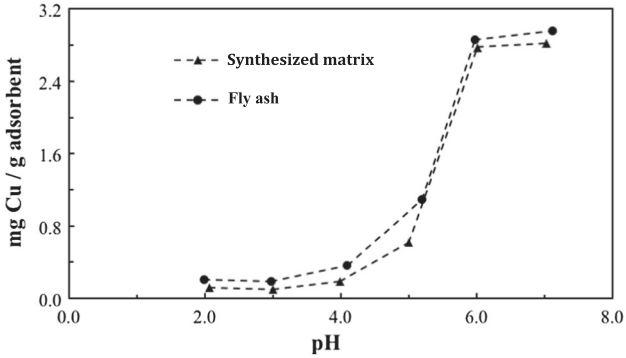

Fig. 5. Effect of pH on the adsorption of Cu^{2+} on fly ash and synthesized matrix.

adsorption of Cu^{2+} on fly ash and synthesized matrix was found between pH 5 and 5.8; at pH > 6 the weak removal of Cu^{2+} resulting from the precipitation of copper species such as hydroxides or carbonates (Fig. 5) must be considered, in accordance with the distribution of metal species as a function of pH [31].

The synthetic matrix was functionalized with an amino group allowing the formation of a complex amino-copper with a stability constant suitable for the formation of the complex. The stability of complex depends on pH value that must be close to the neutrality (10); at pH < 4 the H^+ can join the electronic lone pair of nitrogen preventing the binding of the copper ion with amino group and, at pH > 6 the formation of species leads to the precipitation of copper.

3.2.3. Maximum load capacity

Fig. 6 shows the difference between the load capacity of fly ash and the synthesized material. The fly ash becomes saturated after the second contact, while the synthesized material shows a regular increase in the adsorption capacity as the number of contacts increases. The BET analysis (Table 2) shows an increase of the porosity of the modified material, thus increasing the availability of the active surface, which in turn allows an increase of the adsorption capacity for the metal ion. As seen in Fig. 6, at the fifth contact the synthesized material showed a high loading capacity of 4.1 mg g^{-1} without reaching yet the saturation condition, whereas the fly ash became saturated at the second contact only, with a maximum load of only 3.0 mg g^{-1}.

3.2.4. Contact time and adsorbent mass

The percentage removal of Cu^{2+} by the modified ash with respect to the contact time between the phases was evaluated. Fig. 7 shows the results of three tests with different adsorbent masses; the greatest adsorption efficiency took place

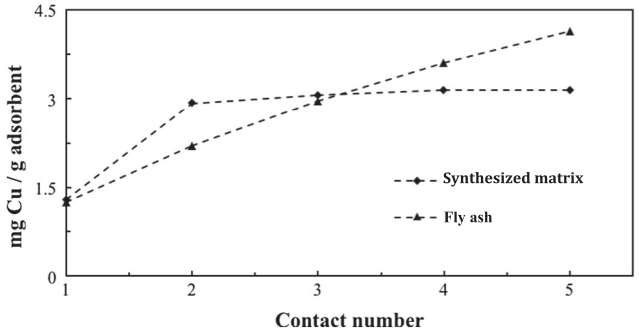

Fig. 6. Comparison between adsorption capacity of fly ash and synthesized matrix, as a function of the number of contacts.

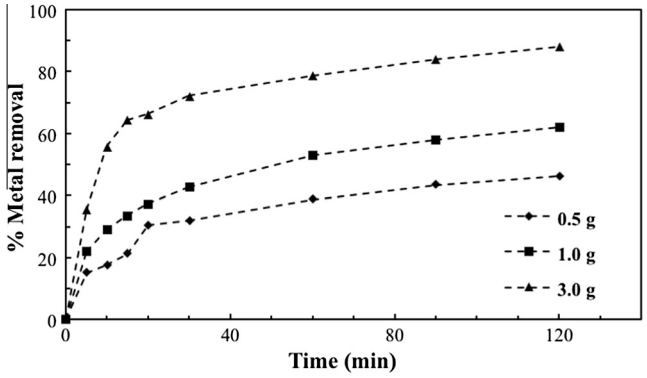

Fig. 7. Variation of adsorbent capacity of synthesized matrix as a function of time at different adsorbent masses.

approximately within 20 min, when 0.5, 1.0 and 3.0 g of adsorbent could remove 30%, 37% and 66% of the metal in solution, respectively. The higher adsorption rate is very likely due to the increased number of active sites as a result of the increased surface area and pore volume of the synthesized material (Table 2). It appears that the adsorption process takes place rapidly and is controlled by diffusion from the bulk of the liquid to the surface of the adsorbent as proposed in reference [32]. After 20 min of contact, the adsorption efficiency of each of the studied masses decreases gradually, probably due to the decrease in the number of active sites on the surface of the synthesized material and to the diffusion of Cu^{2+} in the pores of the material [33]. It has been suggested that this phenomenon may be accounted for by the channel-like structure within the pores with hexagonal symmetry [10], which have a large volume available. During the diffusion process, metal ions initially occupy the sites close to the surface, interfering with the diffusion of the non adsorbed ions into the channels, causing a decrease of the adsorption rate.

4. Conclusion

The Cu^{2+} adsorption capacity of a new material synthesized from coal fly ash was studied under different conditions of pH, initial metal concentrations, maximum load capacity, and contact times for different adsorbent masses. When compared with the initial fly ash, the synthesized matrix showed a greater number of active sites, a much larger specific surface area and pore volume as a result of the functionalization of the mesoporous material with APS. The new material showed great affinity for Cu^{2+}, whose removal was between 95% and 98% for the metal ion concentration range covered in this study. The adsorption model that presented the best fit with the experimental results was that of Freundlich. At pH > 4, there was a fast adsorption rate of Cu^{2+} up to pH 6. At pH > 6 an efficient removal of copper ions was observed, likely attributable to precipitation. The distribution of copper ion species as a function of pH indeed suggests the eventual formation of copper species that can precipitate at those pH. The synthesized matrix was more efficient as the number of contacts increases, compared with the fly ash that becomes saturated at the second contact. With up to 20 min of contact time, the modified fly ash removed the adsorbate rapidly due to the active sites on the surface of the synthesized matrix, so the percentage removal of Cu^{2+} decreased because the diffusion of the metal in the pores became slower.

Acknowledgments

The authors acknowledge the financial support of this project by Innova-Chile, Corfo Code 12IDL2-13631 and by Dicyt Asociativo-Usach code 041331CC_DAS. We thank E. Appiah-Hagan and K. Chartrand who performed the BET and FTIR analysis, respectively.

References

[1] Yao ZT, Xia MS, Sarker PK, Chen T. A review of the alumina recovery from coal fly ash, with a focus in China. Fuel 2014;120:74–85.
[2] Mueller SF, Mallard JW, Mao Q, Shaw SL. Fugitive particulate emission factors for dry fly ash disposal. J Air Waste Manage Assoc 2013;63:806–18.
[3] Soodan RK, Pakade YB, Nagpal A, Katnoria JK. Analytical techniques for estimation of heavy metals in soil ecosystem: a tabulated review. Talanta 2014;125:405–10.
[4] Ahmaruzzaman M. Role of fly ash in the removal of organic pollutants from wastewater. Energy Fuel 2009;23:1494–511.
[5] Blissett RS, Rowson NA. A review of the multi-component utilization of coal fly ash. Fuel 2012;97:1–23.
[6] Gupta VK, Ali I. Utilization of bagasse fly ash (a sugar industry waste) for the removal of cooper and zinc from wastewater. Sep Purif Technol 2000;18:131–40.
[7] Srivastava VC, Mall ID, Mishra IM. Equilibrium modelling of single and binary adsorption of cadmium and nickel onto bagasse fly ash. Chem Eng J 2006;117:79–91.
[8] Cho HC, Oh D, Kim K. A study on removal characteristics of heavy metals from aqueous solution by fly ash. J Hazard Mater 2005;127:187–95.
[9] Pehlivan E, Cetin S, Yank BH. Equilibrium studies for the sorption of zinc and copper from aqueous solutions using sugar beet pulp and fly ash. J Hazard Mater 2006;135:193–9.
[10] Walcarius A, Mercier L. Mesoporous organosilica adsorbents: nanoengineered materials for removal of organic and inorganic pollutants. J Mater Chem 2010;20:4478–511.
[11] Cao J, Wu Y, Jin Y, Yilihan P, Huang W. Response surface methodology approach for optimization of the removal of chromium (VI) by NH2-MCM-41. J Taiwan Inst Chem E 2014;45:860–8.
[12] Silva FAB, Pissetti FL. Adsorption of cadmium ions on thiol or sulfonic-functionalized poly (dimethylsiloxane) networks. J Colloid Interface Sci 2014;416:95–100.
[13] Arsuaga JM, Aguado J, Arencibia A, López-Gutiérrez MS. Aqueous mercury adsorption in a fixed bed column of thiol functionalized mesoporous silica. Adsorption 2014;20:311–9.
[14] Fotoohi B, Mercier L. Recovery of precious metals from ammoniacal thiosulfate solutions by hybrid mesoporous silica: 1-Factors affecting gold adsorption. Sep Purif Technol 2014;127:84–96.
[15] Tapaswi PK, Moorthy MS, Park SS, Ha C-S. Fast, selective adsorption of Cu^{2+} from aqueous mixed metalions solution using 1, 4, 7-triazacyclononane modified SBA-15 silica adsorbent (SBA-TACN). J Solid State Chem 2014;211:191–9.
[16] Jazi MB, Arshadi M, Amiri MJ, Gil A. Kinetic and thermodynamic investigations of Pb(II) and Cd(II) adsorption on nanoscale organo-functionalized SiO_2-Al_2O_3. J Colloid Interface Sci 2014;422:16–24.
[17] Yang H, Chen Y, Feng Q, Li X. Application of amino-functionalized mesoporous silica coated quartz sand for removal of iron and manganese ions from coal mine drainage. Fresen Environ Bull 2013;22:3301–7.
[18] Lam KF, Fong CM, Yeung KL, Mckay G. Selective adsorption of gold from complex mixtures using mesoporous adsorbents. Chem Eng J 2008;145:185–95.
[19] Lam KF, Fong CM, Yeung KL. Separation of precious metals using selective mesoporous adsorbents. Gold Bull 2007;40:192–8.
[20] Abughusa A, Amaratunga L, Mercier L. Extraction of precious metal ions from simulated mine effluents using a nanostructured adsorbent. Can Metall Quart 2006;45:237–41.
[21] Pizarro J, Vergara PM, Rodríguez JA, Valenzuela AM. Heavy metals in northern Chilean rivers: spatial variation and temporal trends. J Hazard Mater 2010;181:747–54.
[22] C09.24. Especificación normalizada para ceniza volante de carbón y puzolana natural en crudo o calcinada para uso en concreto. ASTM Standard; 04.02 2012. C618–12a.
[23] Sing KSW, Everett DH, Haul RAW, Moscou L, Pierotti RA, Rouquerol J, et al. Reporting physisorption data for gas/solid systems with special reference to the determination of surface area and porosity. Pure Appl Chem 1985;57:603–19.
[24] Machida M, Fotoohi B, Amamo Y, Ohba T, Kanoh H, Mercier L. Cadmium (II) adsorption using functional mesoporous silica and activated carbon. J Hazard Mater 2012;221–222:220–7.
[25] Langmuir I. The adsorption of gases on plane surfaces of glass, mica and platinum. J Am Chem Soc 1928;40:1361–403.
[26] Freundlich HMF. Over the adsorption in solution. J Phys Chem-US 1906;57:385–471.
[27] Slejko F. Adsorption technology: a step-by-step approach to process. New York: Eva Appl Marcel Dekker; 1985.
[28] Sari A, Tuzen M, Citak D, Soylak. Equilibrium, kinetic and thermodynamic studies of adsorption of Pb(II) from aqueous solution onto Turkish kaolinite clay. J Hazard Mater 2007;149:283–91.

[29] Cetin S, Pehlivan E. The use of fly ash as a low cost, environmentally friendly alternative to activated carbon for the removal of heavy metals from aqueous solutions. Colloid Surf A 2007;298:83–7.
[30] Dawodu FA, Akpomie GK, Ogbu IC. Application of kinetic rate equations on the removal of copper (II) ions by adsorption unto Aloji Kaolinite clay mineral. Int J Multidisc Sci Eng 2012;3:21–6.
[31] Stumm W, Morgan JJ. Aquatic chemistry: chemical equilibria rates in natural waters. New York: Wiley; 1996.
[32] Das B, Mondal NK. Calcareous soil as a new adsorbent to remove lead from aqueous solution: equilibrium, kinetic and thermodynamic study. UJERT 2011;1:515–30.
[33] Argun ME, Dursun S, Ozdemir C, Karatas M. Heavy metal adsorption by modified oak sawdust, thermodynamics and kinetics. J Hazard Mater 2007;141:77–85.